

Novel Multiferroic State of $\text{Eu}_{1-x}\text{Y}_x\text{MnO}_3$ in High Magnetic Fields

M. Tokunaga,^{1,*} Y. Yamasaki,² Y. Onose,^{2,3} M. Mochizuki,³ N. Furukawa,^{3,4} and Y. Tokura^{2,3,5}

¹The Institute for Solid State Physics (ISSP), The University of Tokyo, Chiba 277-8581, Japan

²Department of Applied Physics, The University of Tokyo, Tokyo 113-8656, Japan

³Multiferroics Project, ERATO, Japan Science and Technology Agency, Tokyo 113-8656, Japan

⁴Department of Physics and Mathematics, Aoyama Gakuin University, Sagami-hara, Kanagawa 229-8558, Japan

⁵Cross-Correlated Materials Research Group, RIKEN, Saitama 351-0198, Japan

(Received 8 June 2008; published 28 October 2009)

Magnetic and dielectric properties of $\text{Eu}_{1-x}\text{Y}_x\text{MnO}_3$ ($x = 0$ and 0.4) are studied in pulsed magnetic fields up to 55 T. For $x = 0$, application of magnetic fields higher than 20 T along the b axis causes magnetic transitions accompanied by generation of electric polarization (P) along the a axis. Similar first-order transitions are also observed in crystals of $x = 0.4$, in which the ground state at zero magnetic field is already a ferroelectric $P \parallel a$ phase of different origin. Realistic model calculation indicates the presence of a novel multiferroic state induced by the spin exchange striction mechanism in high magnetic fields as an essential nature of the frustrated Mn spin system in this class of manganites.

DOI: 10.1103/PhysRevLett.103.187202

PACS numbers: 75.80.+q, 75.30.Kz

Discovery of gigantic magnetoelectric effects in TbMnO_3 [1] shed a new light on the physics of ferroelectric magnets. For materials in which ferroelectricity sets in simultaneously with a magnetic transition, the direct coupling between magnetic and dielectric phases enables us to control the electric polarization (P) by the application of magnetic field (H). Recent theoretical studies pointed out the conditions sufficient for spin structures to accommodate ferroelectricity from the phenomenological [2] and microscopic [3,4] points of view. These prescriptions stimulate magnetoelectric measurements in magnets with a spiral spin structure and lead to the discovery of versatile multiferroic materials [5–8].

Although a number of studies have focused on this issue, the origin of the H -induced change of the P in orthorhombically distorted RMnO_3 has been unclear because the presence of magnetic moments in the rare-earth-metal ions (R) complicates the system. Attempts to use a mixture of nonmagnetic Eu^{3+} and Y^{3+} ions have been carried out to eliminate this difficulty and have succeeded in reproducing the multiferroic phase by tuning the average ionic radius of the A site [9–11]. In this compound, we can investigate the essential effects of the frustrated manganese spin system without magnetic R ions. In $\text{Eu}_{0.6}\text{Y}_{0.4}\text{MnO}_3$, application of H along the a axis (in the P_{bnm} notation) flops the P from the a to the c axis accompanied by the flop in the rotational plane in the cycloidal spin structure [9,11]. Magnetic fields along the c axis stabilize the canted antiferromagnetic (CAF) state with the spontaneous magnetization along the c axis, and, as a result, the P disappears [10,12]. These magnetoelectric phase transitions meet with the intuitive interpretation as a reduction in the Zeeman energy in magnetic system in which accompanying P is derived from the summation of the spin helicities. On the other hand, effects of $H \parallel b$ are veiled in mystery. Application of high magnetic fields along the b axis real-

izes the field-induced multiferroic state in EuMnO_3 [13], whereas the underlying magnetic structure remains unclear. Here, we demonstrate the magnetic and dielectric properties of $\text{Eu}_{1-x}\text{Y}_x\text{MnO}_3$ in higher magnetic fields and argue the existence of a novel multiferroic state in RMnO_3 based on the results of model calculation.

Single crystals of $\text{Eu}_{1-x}\text{Y}_x\text{MnO}_3$ ($x = 0$ and 0.4) were grown by the floating-zone method. Pulsed magnetic fields up to 55 T were generated with a duration time of 36 ms, using nondestructive magnets in the International MegaGauss Science Laboratory of ISSP, The University of Tokyo. Magnetization (M) was measured by induction, using coaxial pick-up coils. Magnetic field-induced changes in P were detected by measuring polarization current [14], which was integrated numerically to obtain the values of P .

In zero field, EuMnO_3 shows successive magnetic phase transitions with decreasing temperature; collinear sinusoidal spin ordering at 51 K and then canted-antiferromagnetic ordering at 46 K. The spontaneous P is not observed in either state. Application of high magnetic fields along the hard magnetization axis (b axis), however, induces P parallel to the a axis [Fig. 1(a)]. The observed values of $P \sim 400 \mu\text{C}/\text{m}^2$ are roughly 30 times larger than those reported earlier [13]. This discrepancy can be ascribed to the difference in the degree of domain orientation. Since the ferroelectric phase appears only in high magnetic fields, we cannot employ the standard electric-field cooling procedure to align the ferroelectric domains. Instead, we studied the H dependence of P in the presence of electric fields (E). Through the P - H curves at various E , we extracted the ferroelectric-like relation between P and E at a constant H (not shown).

We carried out polarization-current measurements for 3×3 directional combinations up to 30 T— $P \parallel \alpha$ - $H \parallel \beta$ with $\alpha, \beta = (a, b, c)$. The results indicate that the field-

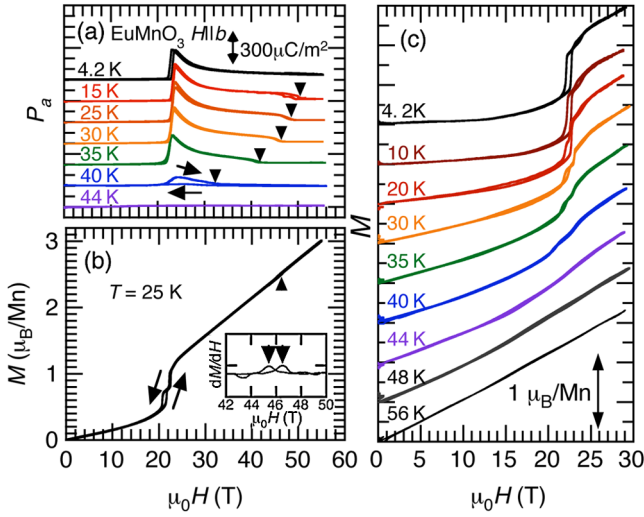


FIG. 1 (color online). (a) Electric polarization parallel to the a axis at various temperatures as a function of applied magnetic fields along the b axis. The P - H curve for each temperature was offset for clarity. Electric fields of 1.4 MV/m were applied during the measurements. (b) Magnetization curve of EuMnO_3 at 25 K. Inset shows the expanded view of differential susceptibility at high field. (c) Magnetization curves up to 30 T at various temperatures. The data are offset for clarity.

induced P appears only in the $P \parallel a$ - $H \parallel b$ configuration. In this direction, a further increase in $H \parallel b$ causes a steep reduction in P with a discernible hysteresis as marked by the triangles in Fig. 1(a). As the temperature increases, the lower and higher transition fields approach each other, and at 44 K, it appears to merge and become undistinguishable.

To clarify the magnetic aspects of this transition, we measured magnetization (M) in $H \parallel b$. Figure 1(b) shows an M - H curve up to 55 T at $T = 25$ K. A steep increase in M is observed at around 22 T, which coincides with the transition to the ferroelectric $P \parallel a$ phase. At around 46 T, we see another anomaly in the M - H curve. This is clear in the differential susceptibility (dM/dH) shown in the inset. Peaks in the dM/dH , i.e., jumps in the M , accompanied by a hysteresis indicate the presence of a first-order transition in this field. The M reaches about $3\mu_B/\text{Mn}$ at 55 T. Judging from the linear behavior of the M - H curves above the transition field, we conclude that Eu ions remain non-magnetic [9] even in this high-field region. Figure 1(c) demonstrates M - H curves up to 30 T at various temperatures. The two-stage jump of M at around 30 K is observed in several samples, and hence could be intrinsic to EuMnO_3 although the origin remains unclear.

To elucidate the nature of the field-induced $P \parallel a$ phase, polarization-current, and magnetization measurements were also performed for $\text{Eu}_{0.6}\text{Y}_{0.4}\text{MnO}_3$, in which the $P \parallel a$ phase is already realized below 24 K in zero magnetic field. Figure 2(a) shows P - H curves at various temperatures. In the present study, we measured the relative change in P with respect to the value at $H = 0$ and did not determine

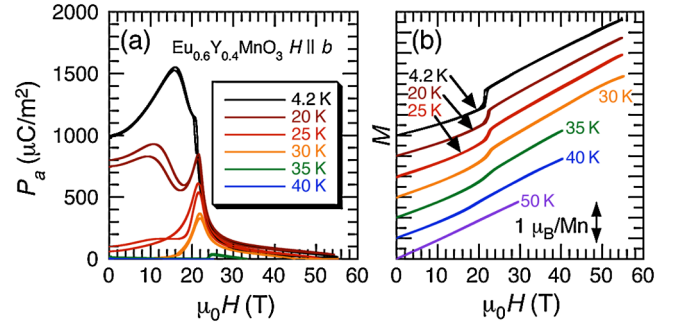


FIG. 2 (color online). (a) Magnetic field dependence of $P \parallel a$ in $\text{Eu}_{0.6}\text{Y}_{0.4}\text{MnO}_3$ at various temperatures. Electric fields of 270 kV/m were applied during the measurements. The vertical axes are offset so that P approaches zero in high-field limit. (b) Magnetization curves at various temperatures for $H \parallel b$. The M - H curves are offset for clarity.

the initial value. The data shown in Fig. 2(a) are offset so that P approaches zero in the high-field limit. The P at zero field as thus determined is in reasonable agreement with those in early reports [9,11]. At 4.2 K, the application of $H \parallel b$ first increases and then decreases P_a while showing a broad maximum at around 16 T. Above 21 T, the P - H curve changes its slope steeply to a downward convex profile similar to that seen in EuMnO_3 . At 30 K, $H \parallel b$ induces a transition from the paraelectric to the ferroelectric phase at around 20 T. The systematic smooth change in P , as functions of H and T , suggests that the high-field $P \parallel a$ state at low temperatures extends up to 35 K. Magnetization measurements revealed that the change of P in $\text{Eu}_{0.6}\text{Y}_{0.4}\text{MnO}_3$ is also accompanied by a steep change in M [Fig. 2(b)]. The presence of the first-order transition indicates the existence of two different $P \parallel a$ phases in this material; the low-field phase below 22 T, known as the ab -plane cycloidal spin state [11], and the high-field one above 22 T. The transition field and the variation of M are similar in $\text{Eu}_{0.6}\text{Y}_{0.4}\text{MnO}_3$ and EuMnO_3 , despite the difference in low-field phases between the compounds.

Electromagnetic phase diagrams of (a) EuMnO_3 and (b) $\text{Eu}_{0.6}\text{Y}_{0.4}\text{MnO}_3$ are shown in Fig. 3. As discussed, the high-field $P \parallel a$ phase (P_a -II) should be distinguished from the $P \parallel a$ phase in low fields (P_a -I). Judging from the similarity in the M - H and P - H curves, we consider that the $P \parallel a$ phase in EuMnO_3 shares the same origin with the P_a -II phase in $\text{Eu}_{0.6}\text{Y}_{0.4}\text{MnO}_3$. The P_a -II phase extends over a wide range of T , irrespective of difference in the underlying low-field phases, such as weakly ferromagnetic, ab - or bc -cycloidal, and sinusoidal collinear phases.

Hereafter, to interpret the origin of the new high-field multiferroic phase (P_a -II) and its disappearance in higher fields, we discuss the magnetic structure in $\text{Eu}_{0.6}\text{Y}_{0.4}\text{MnO}_3$ with use of a classical Heisenberg model. In the theoretical model, the Mn $S = 2$ spins are treated as classical vectors, and the single-ion anisotropy (SIA) and the Dzyaloshinskii-Moriya (DM) interaction as well as the competing super-

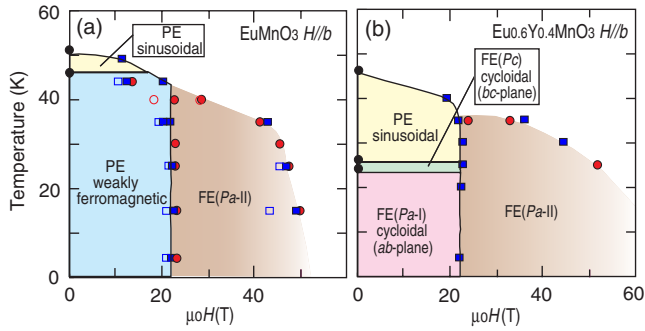


FIG. 3 (color online). Magnetoelectric phase diagrams of (a) EuMnO_3 and (b) $\text{Eu}_{0.6}\text{Y}_{0.4}\text{MnO}_3$ in the H_b - T plane. Circles (squares) represent transition fields determined by the inflection points of the P - H (M - H) curves. Solid and open symbols denote transition fields in field-increasing and decreasing processes, respectively. Solid lines are the guide to the eyes.

exchange interactions are incorporated. This model has been proven to reproduce well all the experimental phase diagrams of RMnO_3 in the absence of magnetic field, as reported in detail in Refs. [15,16]. The parameters used in the calculation are summarized in Table I [16]. We study the thermodynamic properties using the replica exchange Monte Carlo method [17] for a system with $48 \times 48 \times 6$ sites under the periodic boundary condition. On the other hand, the ground-state properties are studied by minimizing the energy.

We display the theoretical T - H_b diagram for $\text{Eu}_{0.6}\text{Y}_{0.4}\text{MnO}_3$ in Fig. 4(a), which reproduces the experimental one in Fig. 3(b). Our analysis has succeeded in reproducing the experiments for $H \parallel a$ and $H \parallel c$ as well, which will be reported elsewhere. Phases I_b and II_b in Fig. 4(a) are identical to the two ferroelectric phases P_a -I and P_a -II in Fig. 3(b), respectively, as will be shown below.

The magnetic structure in each phase can be identified by calculating the spin and spin-helicity correlation functions (not shown). In phase I_b , the Mn spins rotate conically and propagate along b as shown in Fig. 4(b). The

TABLE I. Model parameters used in the calculations. The energy unit is meV. Here \mathcal{H}_{ex} , \mathcal{H}_{sia} , and \mathcal{H}_{DM} are terms of the Hamiltonian, and denote the superexchange, the single-ion anisotropy, and the Dzyaloshinskii-Moriya (DM) interaction terms, respectively. J_{ab} , J_2 , and J_c are the in-plane nearest-neighbor *ferromagnetic* exchange, the next-neighbor *antiferromagnetic* exchange along b and the inter-plane nearest-neighbor *antiferromagnetic* exchange, respectively. D and E express the strength of single-ion anisotropy. α_{ab} , β_{ab} , and γ_{ab} (α_c , β_c , and γ_c) represent the a , b , and c components of DM vectors on the in-plane (inter-plane) Mn-O-Mn bonds.

\mathcal{H}_{ex}	$J_{ab} = -0.80,$	$J_2 = 0.65$	$J_c = 1.25$
\mathcal{H}_{sia}	$D = 0.20,$	$E = 0.25$	
\mathcal{H}_{DM}	$\alpha_{ab} = 0.10,$	$\beta_{ab} = 0.10,$	$\gamma_{ab} = 0.12$
	$\alpha_c = 0.36,$	$\beta_c = 0.56,$	$\gamma_c = 0.0$

conical axes are declined from the c axis towards the b axis. Their c components are aligned ferromagnetically in the ab plane, but antiferromagnetically along the c axis due to the DM vectors on the out-of-plane Mn-O-Mn bonds. The spins rotate approximately within the ab plane with a propagation wave number $q_b = 0.292$. They generate a ferro component of the spin helicities ($\mathbf{S}_i \times \mathbf{S}_{i+b}$) in the c direction, and thereby induce $P \parallel a$ via the inverse DM mechanism.

On the other hand, the spin structure in Phase II_b is similar to that of Phase I_b , but is no longer conical. Instead, the spins form a fan with sinusoidally modulated spin a components [see Fig. 4(c)]. With further increasing H_b , the system enters into Phase III_b , and the sinusoidally modulated spin a components vanish [see Fig. 4(d)].

Importantly, the wave number q_b is commensurate $q_b = 0.25$ in Phase II_b , whereas $q_b = 0.292$ in Phase I_b . This means that the magnetic transition from I_b to II_b is accompanied by an incommensurate-commensurate transition, or a lock-in transition. The magnetic order in Phase II_b has an eight-times periodicity along the x and y bonds. We display arrangement of the sinusoidally modulated spin a components in Phase II_b at $T = 0$ in Fig. 4(e). Concerning their sign, $(++++-- --)$ type order is realized. In this

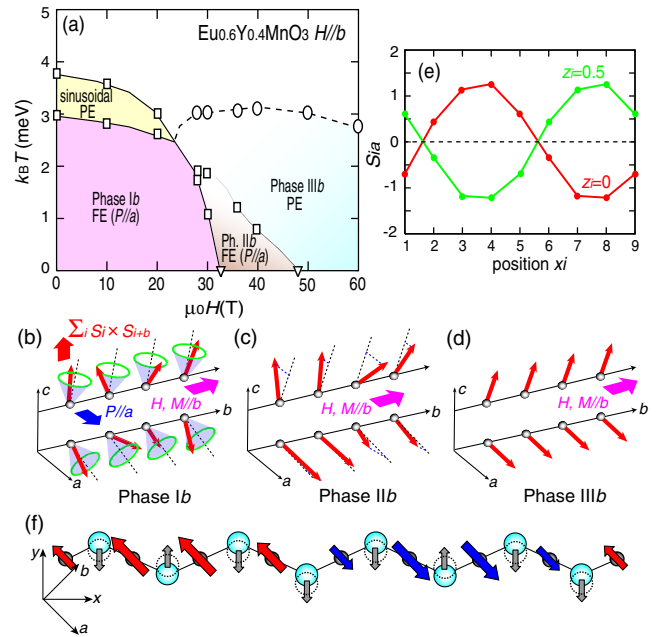


FIG. 4 (color online). (a) Theoretical T - H phase diagram of $\text{Eu}_{0.4}\text{Y}_{0.6}\text{MnO}_3$ under $H \parallel b$. (b)–(d) Spin configurations of phases I_b – III_b and II_b are ferroelectric (FE) with $P \parallel a$, but the origin is different. Other phases are paraelectric (PE). (e) Arrangement of the spin a components on the zigzag Mn-O-Mn-O bond along x . Here, the orthorhombic unit cell contains two MnO planes with $z_i = 0$ and $z_i = 0.5$. (f) Thick arrows represent the a components of spins in the Mn ions. Displacements of the oxygens due to the spin alignment are also shown by thin arrows.

situation, we expect a net electric polarization along the a axis via the symmetric exchange-striction mechanism.

In the perovskite manganites, the spin-exchange interaction is severely affected by the Mn-O-Mn bond angle. Conversely, the Mn-O-Mn bond angle should be more or less modified by the spin alignment. The modification of the oxygen positions caused by the alignment of spin a components in Phase II_{*b*} is demonstrated in Fig. 4(f). Here, the oxygen ions before displacement are represented by solid circles, and those after displacement are predicted by dotted circles. Ferromagnetic (antiferromagnetic) coupling between two neighboring Mn spins in the ab plane becomes stronger as the Mn-O-Mn bond angle increases (decreases). The inverse effect should increase (decrease) the angle of Mn-O-Mn bond with ferromagnetically (antiferromagnetically) aligned neighboring Mn spins. In the zigzag Mn-O-Mn-O- chain along the x axis, the oxygen ions between positive and negative spin a components shift in the same direction. As a result, the oxygen displacements generate P in the $-y$ direction. On the other hand, in the chain along the y axis, P in the $+x$ direction is generated. These two contributions eventually give rise to the net polarization $P \parallel a$ as observed for Phase II_{*b*}. Note that the c components of the local polarizations, if any, are necessarily canceled out because of the presence of mirror plane between the two MnO₂ planes.

Note that the regime of Phase II_{*b*} in the theoretical diagram is rather small as compared to that of the experimental P_a -II phase. This is because our calculation neglects the spin-lattice coupling, and thereby underestimate the area. A commensurate order like Phase II_{*b*} couple to the lattice strongly in reality, which is expected to favor the ordering. Thus, the regime should spread over a wider area with respect to both T and H if we properly take the spin-lattice coupling into account.

In conclusion, we studied the dielectric and magnetic properties of EuMnO₃ and Eu_{0.6}Y_{0.4}MnO₃ in magnetic fields up to 55 T. In both crystals, magnetic fields parallel to the b axis induce magnetic transitions to a multiferroic phase. Model calculation indicates a commensurate spin structure in this high-field phase in which the electric polarization is caused by the symmetric exchange-striction mechanism as contrasted by the low-field spin-cycloidal phase with the inverse Dzyaloshinskii-Moriya interaction induced polarization.

The authors are grateful to K. Kindo and his coworkers for technical assistance provided during experiments on

pulsed magnetic fields. This work was supported in part by a Grant-in-Aid for Scientific Research on priority Areas “High Field Spin Science in 100T” (No. 451) from the Ministry of Education, Culture, Sports, Science and Technology (MEXT).

*tokunaga@issp.t.u-tokyo.ac.jp

- [1] T. Kimura, T. Goto, H. Shintani, K. Ishizaka, T. Arima, and Y. Tokura, *Nature* (London) **426**, 55 (2003).
- [2] M. Mostovoy, *Phys. Rev. Lett.* **96**, 067601 (2006).
- [3] H. Katsura, N. Nagaosa, and A. V. Balatsky, *Phys. Rev. Lett.* **95**, 057205 (2005).
- [4] I. A. Sergienko and E. Dagotto, *Phys. Rev. B* **73**, 094434 (2006).
- [5] G. Lawes, A. B. Harris, T. Kimura, N. Rogado, R. J. Cava, A. Aharony, O. Entin-Wohlman, T. Yildirim, M. Kenzelmann, C. Broholm, and A. P. Ramirez, *Phys. Rev. Lett.* **95**, 087205 (2005).
- [6] K. Taniguchi, N. Abe, T. Takenobu, Y. Iwasa, and T. Arima, *Phys. Rev. Lett.* **97**, 097203 (2006).
- [7] Y. Yamasaki, S. Miyasaka, Y. Kaneko, J.-P. He, T. Arima, and Y. Tokura, *Phys. Rev. Lett.* **96**, 207204 (2006).
- [8] S. Park, Y. J. Choi, C. L. Zhang, and S.-W. Cheong, *Phys. Rev. Lett.* **98**, 057601 (2007).
- [9] K. Noda, M. Akaki, T. Kikuchi, D. Akahoshi, and H. Kuwahara, *J. Appl. Phys.* **99**, 08S905 (2006).
- [10] J. Hemberger, F. Schrettle, A. Pimenov, P. Lunkenheimer, V. Yu. Ivanov, A. A. Mukhin, A. M. Balbashov, and A. Loidl, *Phys. Rev. B* **75**, 035118 (2007).
- [11] Y. Yamasaki, S. Miyasaka, T. Goto, H. Sagayama, T. Arima, and Y. Tokura, *Phys. Rev. B* **76**, 184418 (2007).
- [12] V. Yu. Ivanov, A. A. Mukhin, V. D. Travkin, A. S. Prokhorov, A. M. Kadomtseva, Yu. F. Popov, G. P. Vorob'ev, K. I. Kamilov, and A. M. Balbashov, *J. Magn. Mater.* **300**, e130 (2006).
- [13] A. M. Kadomtseva, Yu. F. Popov, G. P. Vorob'ev, V. Yu. Ivanov, A. A. Mukhin, and A. M. Balbashov, *Sov. Phys. JETP* **81**, 590 (2005).
- [14] H. Mitamura, S. Mitsuda, S. Kanetsuki, H. A. Katori, T. Sakakibara, and K. Kindo, *J. Phys. Soc. Jpn.* **76**, 094709 (2007).
- [15] M. Mochizuki and N. Furukawa, *J. Phys. Soc. Jpn.* **78**, 053704 (2009).
- [16] M. Mochizuki and N. Furukawa, arXiv:0905.1857.
- [17] K. Hukushima and K. Nemoto, *J. Phys. Soc. Jpn.* **65**, 1604 (1996).